Mirroring Perfection: The Structure of Methylglyoxal Synthase Complexed with the Competitive Inhibitor 2-Phosphoglycolate†

Dana Saadat and David H. T. Harrison*

Department of Biochemistry, Medical College of Wisconsin, 8701 Watertown Plank Road, Milwaukee, Wisconsin 53226

Received November 18, 1999; Revised Manuscript Received December 20, 1999

ABSTRACT: The crystal structure of the transition-state analogue 2-phosphoglycolate (2PG) bound to methylglyoxal synthase (MGS) is presented at a resolution of 2.0 Å. This structure is very similar to the previously determined structure of MGS complexed to formate and phosphate. Since 2PG is a competitive inhibitor of both MGS and triosephosphate isomerase (TIM), the carboxylate groups of each bound 2PG from this structure and the structure of 2PG bound to TIM were used to align and compare the active sites despite differences in their protein folds. The distances between the functional groups of Asp 71, His 98, His 19, and the carboxylate oxygens of the 2PG molecule in MGS are similar to the corresponding distances between the functional groups of Glu 165, His 95, Lys 13, and the carboxylate oxygens of the 2PG molecule in TIM. However, these spatial relationships are enantiomorphic to each other. Consistent with the known stereochemical data, the catalytic base Asp 71 is positioned on the opposite face of the 2PG-carboxylate plane as Glu 165 of TIM. Both His 98 of MGS and His 95 of TIM are in the plane of the carboxylate of 2PG, suggesting that these two residues are homologous in function. While His 19 of MGS and Lys 13 of TIM appear on the opposite face of the 2PG carboxylate plane, their relative location to the 2PG molecule is quite different, suggesting that they probably have different functions. Most remarkably, unlike the coplanar structure found in the 2PG molecule bound to TIM, the torsion angle around the C1−C2 bond of 2PG bound to MGS brings the phosphoryl moiety out of the molecule's carboxylate plane, facilitating elimination. Further, the superimposition of this structure with the structure of MGS bound to formate and phosphate suggests a model for the enzyme bound to the first transition state.

The faithful conversion of substrates to products is a hallmark of enzymatic catalysis (i.e., one enzyme catalyzes one reaction to the near exclusion of all other reactions). Methylglyoxal synthase (MGS) (EC 4.2.99.11) and the "evolutionarily perfect enzyme" (*1*) triosephosphate isomerase (TIM) use the same initial chemical steps to form the enediol(ate) of dihydroxyacetone phosphate (DHAP) to faithfully catalyze the elimination of phosphate and the isomerization of the substrate, respectively. In general, the reaction pathway used by an enzyme gives rise to reactive intermediates that are capable of undergoing a variety of different chemistries. However, the structural basis for how enzymes which produce chemically identical intermediates specify different products has only been extensively studied in enzymes that use pyridoxal-5′-phosphate (PLP) as a cofactor (*2*−*5*). These studies conclude that the enzyme controls the microscopic environment of the cofactor to specify decarboxylation, racemization, or transamination.

Unlike the PLP enzymes, MGS and TIM have no cofactor, yet manage to specify two different products from their common intermediate. In both MGS and TIM, the first step of the reaction mechanism involves the stereospecific abstraction of the C3 hydrogen of DHAP to form a common enediol(ate) enzyme intermediate (eq 1) (*1*, *6*). However,

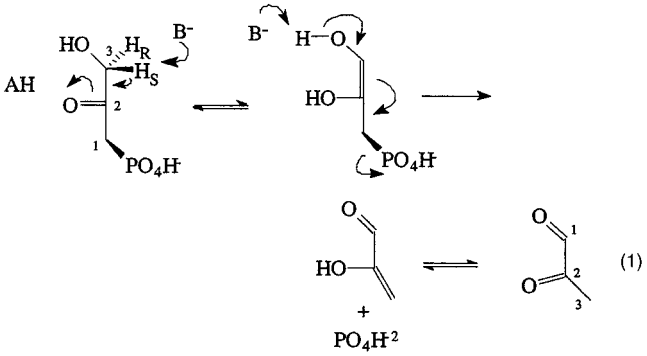

(1)

MGS abstracts the *pro*-S hydrogen, whereas TIM abstracts the *pro*-R hydrogen. MGS then catalyzes the 1,4-β-elimination of the enediol(ate) to form the enol of methylglyoxal and inorganic phosphate, while TIM reprotonates the enediol(ate) intermediate at the C2 position to form glyceraldehyde 3-phosphate (GAP). Both enzymes catalyze their respective reactions with remarkably similar kinetic constants: k_{cat} = 220 s^{-1}, K_m = 0.2 mM, and $k_{cat}/K_m = 1.1 \times 10^6$ M^{-1} s^{-1} for

† This work was supported by the Juvenile Diabetes Foundation International and by NIH DK51697 (to D.H.T.H.).

* To whom correspondence should be addressed. E-mail: harrison@eeyore.biochem.mcw.edu. Phone: (414) 456-4432. Fax: (414) 456-6510.

[1] Abbreviations: MGS, methylglyoxal synthase; TIM, triosephosphate isomerase; DHAP, dihydroxyacetone phosphate; 2PG, 2-phosphoglycolate; PLP, pyridoxal-5′-phosphate; GAP, glyceraldehyde phosphate; NCS, noncrystallographic symmetry; DHAS, dihydroxyacetone sulfate.

10.1021/bi992666f CCC: $19.00
Published on Web 02/25/2000

MGS, and $k_{cat} = 600\ s^{-1}$, $K_m = 0.65$ mM, and k_{cat}/K_m(TIM) $= 9.2 \times 10^5\ M^{-1}\ s^{-1}$ for TIM (*1*, *7*). Despite the similarity in the initial catalytic step, MGS is highly specific for dihydroxyacetone phosphate and is not able to catalyze the elimination reaction using the more reactive D- or L-GAP. Unlike TIM, which catalyzes a uni−uni reaction, MGS catalyzes a uni−bi reaction where the dissociation of the enol aldehyde of methylglyoxal is believed to precede that of inorganic phosphate (*8*). Spectrophotometric evidence (I. A. Rose, personal communication) and the observation that the C-3 position of methylglyoxal is protonated nonstereospecifically (*6*) strongly suggest that the enol aldehyde is the actual product of MGS. This product then tautomerizes in solution to form methylglyoxal.

Methylglyoxal synthase catalyzes the first reaction in the methylglyoxal bypass of the Embden−Myerhoff pathway (glycolysis) (*9*, *10*). The physiological benefits conferred upon bacteria by the methylglyoxal bypass (methylglyoxal synthase and the glyoxalase system) are not well understood. Methylglyoxal, the ultimate product of methylglyoxal synthase, is cytotoxic in millimolar quantities and has been shown to be mutagenic and to interfere with de novo protein and nucleic acid synthesis (*11*−*14*). The *S*-D-lactoylglutathione intermediate of the glyoxalase system is also toxic in millimolar quantities and is known to interfere with the synthesis of intermediate filaments (*15*). Attempts to understand the benefits conferred by methylglyoxal synthase have focused on growth under nonideal conditions. The fact that phosphate acts as an allosteric inhibitor of the enzyme suggests that the methylglyoxal bypass is only active under conditions of phosphate starvation (*16*). However, recent evidence suggests that the role for this microbial enzyme may be to facilitate the transition between conditions of starvation and abundance (*17*). Interest in methylglyoxal metabolism stems in part from the suggestion that methylglyoxal is implicated in diabetic complications (*18*). Further interest comes from the ability of the human glyoxalase system to clear 2-oxo aldehyde-based chemotherapeutic drugs (e.g., methylglyoxal-bis-guanylhydrazone) from tumors, rendering the treatment ineffective (*19*). Commercial interest in methylglyoxal metabolism derives from the potential use of methylglyoxal synthase in engineered microorganisms to produce the industrially important compound 1,2-propanediol (*20*).

Methylglyoxal synthase has been cloned, sequenced, and overexpressed in *Escherichia coli* (*7*, *17*). Sequences homologous to methylglyoxal synthase from several bacterial species indicate the absolute conservation of several charged amino acid residues: Asp 20, Asp 71, Asp 91, Asp 101, Arg 107, His 19 and His 98, and Lys 21. To identify the catalytic base that abstracts the C3 proton, each of the four conserved aspartic acid residues has been mutated to either an asparagine or a glutamic acid (*7*). The steady-state kinetics and the allosteric sensitivity to phosphate for each of the mutant enzymes were characterized. These studies showed that the mutant enzymes D20N and D91N are much less sensitive to phosphate inhibition. The kinetics of the D71N and D101N mutant enzymes showed that k_{cat}/K_m was reduced by 10^3- and 10^4-fold, respectively. A similar decrease was shown when these aspartate residues were replaced by glutamate. The competitive inhibitor 2-phosphoglycolate (2PG, $K_i = 2\ \mu$M, at pH 7.0) was studied with the mutant enzymes to suggest that Asp 71 is the catalytic base that abstracts the proton from the C3 position of DHAP. Additionally, 2PG was used to show that the D71E and D101E mutant enzymes are "locked" in the "taut" conformation.

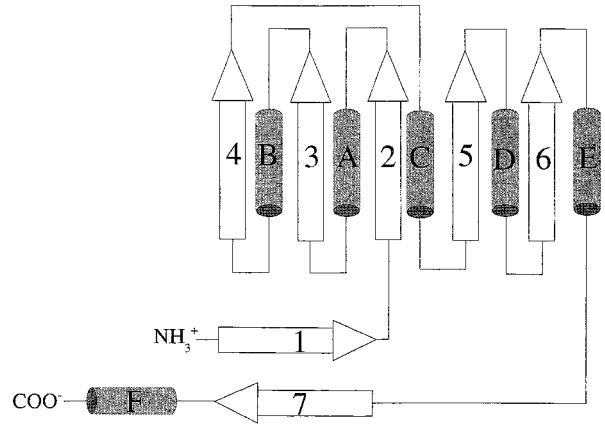

FIGURE 1: Schematic representation of the topology of MGS. The active site is located at the amino-terminus of α helices B and C and at the carboxy-terminus of β strands 2, 3, and 4. A residue from α helix F participates in forming the active site.

The crystal structure of methylglyoxal synthase shows that the enzyme is a homohexamer of subunits that have a core fold of a β/α protein (*21*). The topology of the core is defined by five parallel strands in the order 4−3−2−5−6 with α helices A−E connecting each strand in sequence (Figure 1). The active site of the protein is located at the carboxy end of the parallel β sheet between the second and third β strands and amino termini of α helices B and C. In addition to the core β/α fold, there is a pair of antiparallel β strands that derive from the amino-terminus and carboxy-terminal residues. After this terminal β strand, the carboxy-terminus forms α helix F that interacts with the active site of the neighboring subunit. The structure shows that Asp 101 from α helix D makes an intersubunit salt bridge with Arg 107 also on α helix D. Asp 71 makes a hydrogen bond to a bound formate ion in the active site, which is consistent with our previous suggestion that Asp 71 is the catalytic base (*21*).

The crystal structure of TIM complexed with 2PG ($K_i = 15\ \mu$M, at pH 6.8) shows that the protein folds as an $(\alpha/\beta)_8$ barrel (*22*). It has been proposed that 2PG has the stereochemistry and charge configuration that mimics part of the transition state of the catalytic step that converts DHAP to the enediol(ate) intermediate common to both MGS and TIM. Since the overall fold of TIM is different than that of MGS, it has been difficult to compare the active sites of these two enzymes to understand the similarities and differences in the mechanisms of MGS and TIM. To overcome this difficulty, we have determined the three-dimensional structure of *E. coli* MGS complexed to 2PG. The structures of the active-site pocket of the two enzymes bound to this common transition-state analogue are here compared.

METHODS AND MATERIALS

Protein Purification and Crystallization. Wild-type recombinant MGS was expressed in pETmgswt transformed BL21(DE3) *E. coli* cells and purified as previously reported (*7*). MGS crystals were formed using the sitting drop vapor diffusion method. The crystallization solution consisted of

Table 1: Data Collection Statistics[a]

resolution (Å)	30−2.0
no. of reflections observed ($I/\sigma > 0$)	166 553
no. of reflections unique ($I/\sigma > 0$)	74 981
% complete ($I/\sigma > 0$)	88.8 (63.7)[b]
R_{merge}[c] ($I/\sigma > 0$)	7.0%

[a] Merged data from two different crystals. [b]Completeness in highest resolution shell 2.03−2.0 Å. [c] $R_{merge}(I) = \sum_{hkl}\sum_i|I_i - I_I(hkl)|/\sum_{hkl}\sum_i I_i(hkl)$.

18% PEG 1500 and 100 mM sodium cacodylate (pH 6.5). Crystallization drops were formed by mixing an equal volume of a 25 mg/mL MGS protein solution in 20 mM imidazole-HCl (pH 7.0), 1 mM KH_2PO_4, and 10 mM 2-phosphoglycolate (2PG) with the crystallization solution. The volume of the crystallization drops ranged from 10 to 20 μL. The crystal trays were incubated at room temperature and crystals grew with an average long dimension of over 0.6 mm with a minimum dimension of over 0.3 mm in about 2 weeks. The crystals have an orthorhombic morphology different from the hexagonal crystals grown in the presence of formate and phosphate (*21*).

Data Collection. MGS crystals mounted in oil-sealed 1.0 mm diameter quartz capillaries were centered in a two-circle Rigaku R-axis II image plate detector system and exposed to 0.3 mm collimated graphite monochromatized CuK_α radiation generated from a Rigaku RU-200 rotating anode X-ray generator at 50 kV x 100 mA. Rotation photographs of 1.0 degree were taken with the crystal to detector distance set to 185 mm and a 2θ angle of 17°. Image data were processed (integrated, corrected, and scaled) with the HKL program suite (*23*). One data set was collected from a first crystal and three different data sets where collected from a second crystal by successively translating the crystal along the *z*-axis by 0.2 mm between each data set. The data statistics are presented in Table 1.

Structure Determination. The crystal structure of the MGS/2PG complex was solved by the molecular replacement method using the X-PLOR program (*24*). The initial search model was the hexamer of MGS as it appeared in our previously determined structure (*21*). The phosphate and formate atoms were not included in the search model. Intensity data that were between 10.0 and 4.5 Å resolution and greater than 2.0σ above background were used to conduct a rotation search with this model. The search was restricted to the asymmetric unit using an angular search interval of 2.5°. The rotation function showed six peaks that were related by a 6-fold rotation with a peak height that was significantly above the next highest solution. The solution with the highest rotation function from the rotation search was applied to the search model. The model was then used in the translation function using data between 15.0 and 4.0 Å for a number of orthorhombic space groups. This verified the space group assignment of $P2_12_12_1$. The search was performed in the range $x = 0-0.5$, $y = 0-0.5$, and $z = 0-0.5$.

Structure Refinement. Prior to refinement, 5% of the data between 30.0 and 2.0 Å was set aside for the calculation of R_{free} (*25*) using the program DATAMAN (*26*). These data were selected in 15 discrete resolution shells each containing 249 reflections. This method of selecting the R_{free} set was employed rather than the random selection of reflections to unbias the effects of noncrystallographic symmetry (NCS) (*27*). After rigid body refinement of the model using data between 10 and 4.0 Å resolution, the crystallographic *R*-factor was 33.6%. An electron density map was calculated using model phases and $2|F_0| - |F_C|$ as Fourier coefficients. The map revealed that the phosphate-bound conformation fit well within the electron density for each subunit. A hexameric model of MGS was constructed with all of the subunits in the phosphate-bound conformation. This model was subjected to rigid body refinement using data between 10 and 3.0 Å and the *R*-factor resulting in the decrease of the crystallographic *R*-factor to 30.0%. NCS restraints were imposed between the six subunits from residue 1−151 (weight of 350 Å^2 and 2 sigma for *B*-factor restraints), and the model was subjected to torsion-angle simulated annealing refinement with a starting temperature of 5000 K against data of 8.0−2.0 Å resolution. Alternate rounds of least squares, simulated annealing, and temperature factor refinement were interleaved with manual (re)building using the program O (*28*) until the free *R*-factor converged. Initially, NCS restraints were imposed between all atoms of the six subunits. Using the free *R*-factor as a guide, the NCS restraints were removed for 17% of all of the protein atoms where the electron density showed significant deviation from NCS relationship. The following is a list of residues that were not restrained by NCS: 1−3, 11, 21, 25, 32, 33, 38, 39, 128−139, 151, 152. Furthermore, using the free *R*-factor as a guide, the NCS restraints were relaxed to a final weight of 125 Å^2 and 2σ for *B*-factor restraints.

Electrostatic Calculations. The program DELPHI (*29*) was used to solve the Poison−Boltzman equation for each point on a 65 × 65 × 65 grid which encapsulated the protein. Default assumptions about dielectric constants (80 for solvent, 2 for solute, 0.1 M ionic strength) and a probe size of 1.4 Å were used. Hydrogen atoms were added to the model. Partial charges were assigned to each atom using INSIGHT's consistent valance force field (CVFF). The electrostatic surface potential was built and visualized using the program GRASP (*30*).

Structural Alignment. The program O was used to calculate a least-squares fit of the Cα atom positions between 2PG bound subunit and Pi bound subunits of MGS.

RESULTS

Structure Determination. Crystals of MGS complexed with the competitive inhibitor 2PG were found to be in the space group $P2_12_12_1$ with cell dimensions of $a = 53.1$ Å, $b = 129.9$ Å, and $c = 178.6$ Å. The asymmetric unit consisted of one hexamer of MGS, giving a Matthews coefficient of $V_M = 3.04$ Å^3/Da. The structure was determined by molecular replacement methods (see Methods and Materials). Prior to the additions of nonprotein atoms to the model, but after the application of NCS restraints and simulated annealing refinement, the *R*-factor was 25.7% and the R_{free} was 27.6%. The electron density maps (using either $2|F_0| - |F_C|$ or $|F_0| - |F_C|$ as Fourier coefficients) clearly revealed the presence of the bound 2PG molecule in each active site (Figure 2). These molecules were built into the model. Additionally, about 100 water molecules were identified. The model was subjected to positional refinement with NCS restraints between the six protein subunits. Regions that did not display

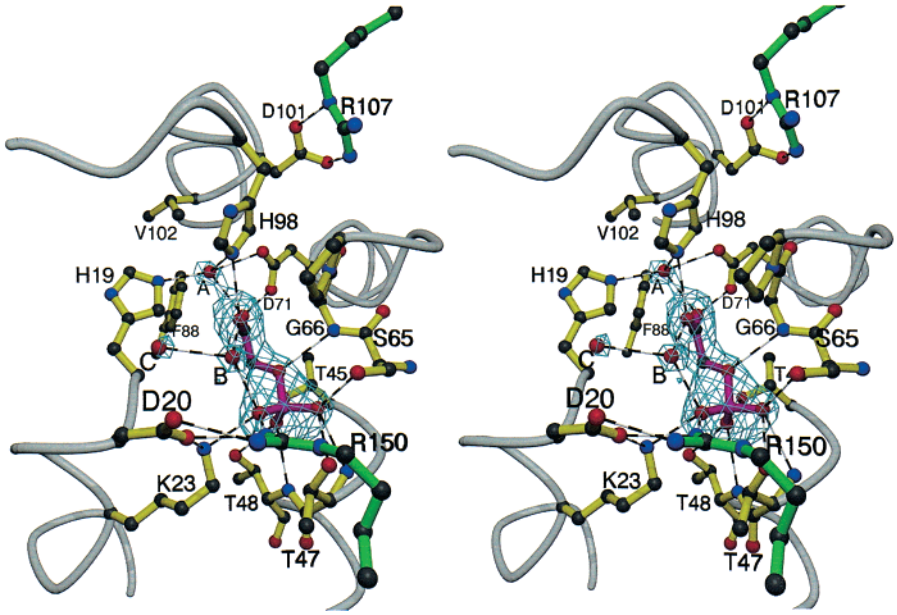

FIGURE 2: Stereoview of the mode of binding of 2PG to the active site of MGS. The $F_{observed} - F_{calculated}$ electron density map (in blue) calculated prior to the placement of the 2PG inhibitor (in magenta) or water molecules (in red) is contoured at the 3σ level. The residues Arg 107 and Arg 150 (in green) are from a symmetry related molecule within the hexamer. Dashed lines represent the potential hydrogen bonds or salt bridges in the active site.

NCS were omitted from the list of atoms to be restrained. After the addition of another 200 water molecules, bulk solvent correction and another two rounds of manual rebuilding, positional refinement, and individual *B*-factor refinement, the *R*-factor was 18.7% and the R_{free} was 21.9% (Table 2). The Ramachandran plot shows that 92.7% of the residues fall within the most favored region.

Comparison to the Previous Structure of MGS. The overall fold of each subunit in the 2PG-bound MGS is very similar to the overall fold of the phosphate-bound form of MGS. The least-squares fit of the Cα atom positions between a 2PG-bound subunit and a phosphate-bound subunit gives a root-mean-square deviation (RMSD) of 0.23 Å, while the RMSD between a 2PG-bound subunit and a phosphate-free subunit is 0.63 Å. As with the comparison between the phosphate-bound and phosphate-free structures, most of the changes can be localized to the region of α helices B and F (*21*). Many of the regions where NCS restraints were not applied (e.g., Arg 32, Asp 134) are part of hexamer−hexamer contacts within this crystal form which cause differences with the previously determined structures.

Active Site. The active site is located in the cleft formed by the loops at the C-terminal of the open β-sheet (Figure 2). The inhibitor 2-phosphoglycolate is bound to the active site of all six subunits in the asymmetric unit. It should be noted that in addition to the electron density surrounding the 2PG molecule, there are three extra spherical pieces of electron density in the active-site labeled A, B, and C. On the basis of their distance from hydrogen-bond donors and acceptors, sites B and C are likely to be water molecules. The electron density at site A is unexplained due to its close proximity to the carboxylate of 2PG (2.6 Å) and to the methyl of Val 102 (3.1 Å), thus it is unlikely to be a water molecule, and its coordination is not typical of a sodium ion.

Since it is not possible at this resolution to determine the locations of protons, literature precedence was followed in proposing an appropriate protonation scheme. The protonation state shown for residue Asp 71 in the active site (Figure 3) is based on the homology found with 2PG bound to TIM, where the Glu 165 has been shown to be protonated in the presence of 2PG (*22*, *31*). The protonation state of the remaining residues in the enediolate binding reflect this choice. It has been pointed out that the protonation state of

Table 2: Crystal Parameters and Refinement Statistics

space group	$P2_12_12_1$
cell dimensions	
a (Å)	53.1
b (Å)	129.9
c (Å)	178.6
protein data bank accession no.	1EGH
σ cut off	2.0
resolution range (high res. shell) (x81)	30.0−2.0 (2.09−2.00)
no. of reflections	68596 (5,451)
completeness	81.2% (69.3%)
free *R*-value	21.9% (29.4%)
R-value	18.7% (27.9%)
no. of protein atoms	6970
no. of water atoms	300
no. of 2-phosphoglycolate atoms	54
Ramachandran most favored/additional (%)[a]	92.3/7.7
overall mean temperature factor (Å^2)	30.6
mean temperature factor for protein atoms (Å^2)	30.0
mean temperature factor for solvent atoms (Å^2)	43.6
RMS deviation from ideality[b]	
bond lengths (Å)	0.006
bond angles (deg)	1.2
dihedral angles (deg)	25.6
improper angles (deg)	0.6

[a] Most favored and additionally allowed regions defined by PROCHECK (*58*). [b]Root-mean-square deviations from Engh and Huber ideal values (*59*).

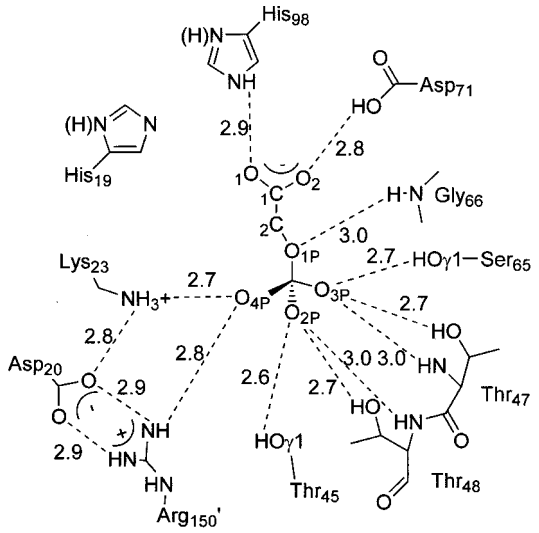

FIGURE 3: Schematic Diagram of the Active Site With 2PG Bound.

Glu 165 in the presence of 2-phosphoglycolate is similar to the protonation state of Glu 165 in the presence of the enediolate, except that the proton must be derived from a solvent molecule instead of the carbon acid (*32*).

The phosphoryl moiety of 2PG sits on top of the N-terminal of helix B making interactions with a variety of ligands in a manner that is identical to those of inorganic phosphate in the related structure. Specifically, the phosphoryl moiety of 2PG is within hydrogen-bonding distance of the Nζ nitrogen of Lys 23, the Oγ oxygen of Thr 45, Thr 47, Thr 48, and Ser 65, and the peptide nitrogen of Thr 47, Thr 48, and Gly 66 (Figure 3). The phosphoryl moiety also interacts with Arg 150′ of a 2-fold symmetry-related subunit which completes the active site. In addition to forming close contacts with the phosphoryl portion of 2PG, the Nϵ2 nitrogen atoms of His 98, and the Oδ1 oxygen of Asp 71 are within hydrogen-bonding distance to the carboxylate of 2PG. With the exception of Arg 150′, each of these residues is conserved across all *mgsA* homologous sequences. The bottom of the active site shows a number of hydrophobic residues that limit and define the size and shape of the substrate molecule.

Conformation of 2PG. The average torsion angles for the 2PG molecule as it is bound to MGS are O3P−P−O1P−C2 177 ± 2°, P−O1P−C2−C1 148 ± 3°, and O1P−C2−C1−O1−57 ± 2°, while the corresponding torsion angles in TIM are 160°, 166°, and 0° (*22*) (see Figure 4a). The O3P−P−O1P−C2 torsion angle for MGS corresponds to the most likely rotamer for an alkyl phosphate, while in TIM, this may represent a high-energy state. The P−O1P−C2−C1 torsion angle for MGS indicates that there is a kink in the alignment of the phosphoryl group with respect to the ethyl moiety, while in TIM, this angle is near the resting state. Lastly, the O1P−C2−C1−O1 torsion angle for MGS indicates that the bridging oxygen is neither in the plane formed by the carboxylate of 2PG nor is it orthogonal to this plane, while in TIM, this angle places the bridging oxygen in the plane of the 2PG carboxylate.

Alignment with Triosephosphate Isomerase. The acetyl moiety of 2PG was used to align the active site of TIM with the active site of MGS (Figure 4a). The comparison of the two active sites and the known stereochemistry of proton abstraction suggested the presence of a pseudo mirror plane corresponding to the carboxylate plane of 2PG. The distances between the carboxylate oxygens of Glu 165 in TIM and the nearest carboxylate oxygen of 2PG are 3.2 and 2.7 Å, respectively (*22*), while the homologous distances from Asp 71 in MGS are 3.4 and 2.8 Å, respectively (Figure 3). Similarly, the distance form Nϵ2 nitrogen of His95 in TIM to the carboxylate oxygen of 2PG corresponding to the carbonyl oxygen of DHAP is 2.7 Å, while the homologous distance from His 98 in MGS is 2.9 Å. The distance from the Nζ nitrogen of Lys 12 in TIM to the same carboxylate oxygen is 3.0 Å, while the corresponding distances from His 19 in MGS for the Nϵ2 nitrogen is 4.2 Å and the Cδ2 carbon is 3.7 Å. A comparison of the electrostatic potential surfaces of MGS and TIM show that the phosphoryl moiety of 2PG is buried in a positively charged pocket in MGS, whereas the phosphoryl moiety is bound to a positively charged cleft that is mostly exposed to solvent when bound to TIM. The carboxylate moiety of 2PG is partially exposed to solvent when bound to MGS; however, the phosphoryl moiety is completely buried in MGS.

DISCUSSION

The elimination of phosphate from triose phosphates has been extensively studied under a number of conditions: in the absence of any catalyst, using buffer catalysts, using triosephosphate isomerase as a catalyst, and using methylglyoxal synthase as a catalyst (*6*, *33*−*37*). These studies all suggest that the first step of the reaction mechanism for DHAP is the loss of a proton at the C3 position to form the enediolate. The enediolate may then be reprotonated at either the C3 or C2 position or the enediolate may collapse to form the enol of methylglyoxal and inorganic phosphate. In the uncatalyzed reaction, the phosphoryl of the triose phosphate acts to catalyze the rate-determining first step of the reaction, yet the elimination of phosphate remains a nonconcerted two-step mechanism (*35*). In the buffer-catalyzed reaction, the rate of enediolate formation is found to be proportional to the basic strength (pK_a) of the buffer (*35*). A Brønsted β value of 0.48 is found for a series of 3-substituted quinuclidine buffers. The unusually small value for β is attributed to the negative charge of the phosphoryl moiety affecting the transition state. Once the enediolate is formed, the rate of reprotonation at the C3 or C2 positions and the state of ionization of the phosphoryl moiety affects the observed rate of elimination. The rate of reprotonation at a given pH is dependent on the pK_a of the buffer; the lower the pK_a, the greater the rate. The rate at which the enediolate collapses and eliminates phosphate is dependent on the ionization state of the phosphoryl moiety. The phosphoryl dianion is about 100 times less effective as a leaving group than is the monoanion under conditions of moderate pH.

Enediol(ate) Formation. The structure of 2PG bound to MGS reveals three important structural features that together allow MGS to catalyze the elimination of phosphate from DHAP to form the enol of methylglyoxal (Figure 2). Recall that in the uncatalyzed and buffer-catalyzed elimination reaction, the formation of the enediolate is rate determining. The MGS structure suggests that the enzyme catalyzes enediol(ate) formation in a manner nearly identical to that of TIM. The catalytically important residue Asp 71 of MGS is positioned at a similar distance to a carboxylate oxygen

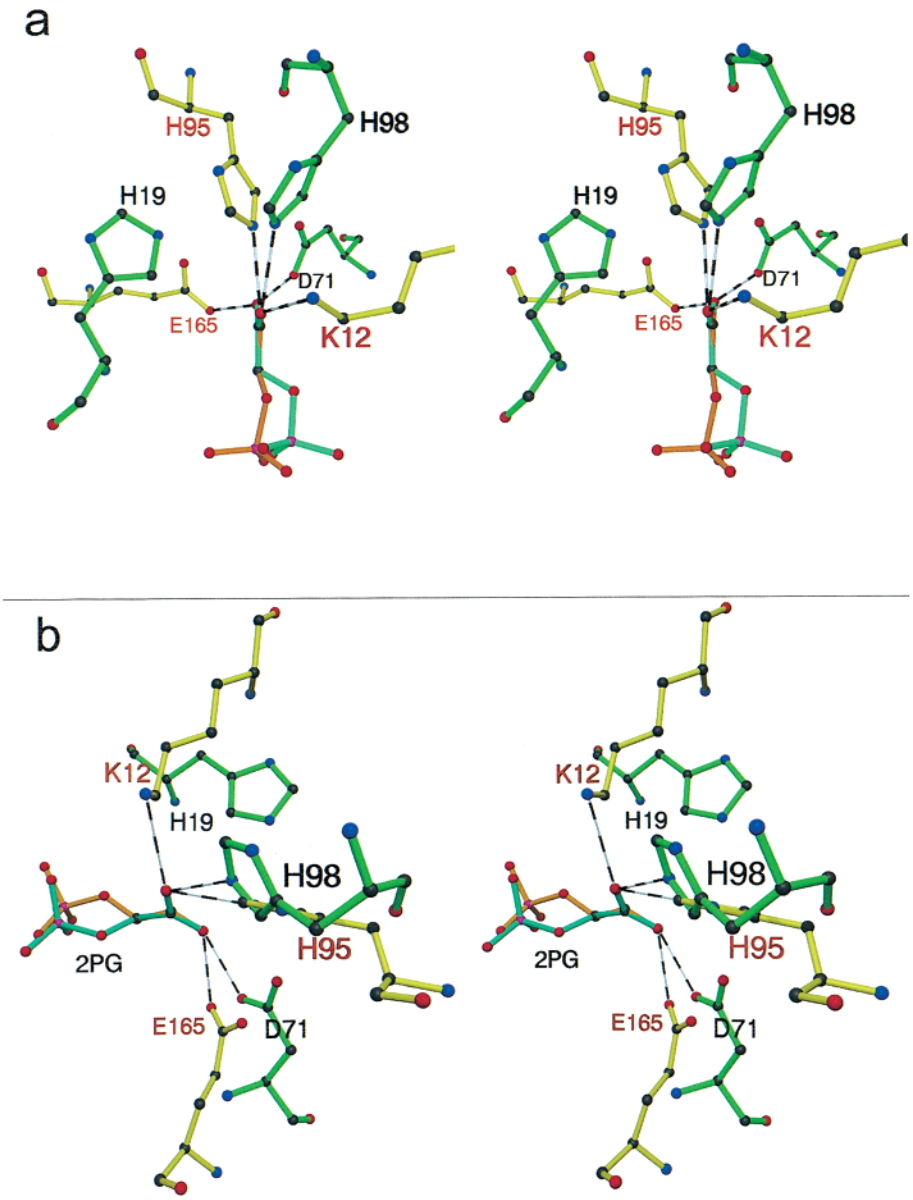

FIGURE 4: Active sites of MGS and TIM. (a) The superimposition of the active sites of MGS (green/aqua) and TIM (yellow/orange) bound to the competitive inhibitor 2PG. The superimposition was achieved by aligning the acetyl moiety of 2PG bound to MGS with the acetyl moiety of 2PG bound to TIM. A pseudo-mirror plane corresponds to the carboxylate plane of 2PG and reveals the enantiomorphic relationship between Glu 165, His 95, and Lys 12 of TIM and Asp 71, His 98, and His 19 of MGS. Note that the bridging oxygen of 2PG in TIM is in the plane of the carboxylate of 2PG whereas it is out of the plane in MGS. (b) The superimposition of MGS and the mirror image of TIM aligned using the acetyl moiety of the bound 2PG molecules. The amino group of Lys 12 in the mirror image TIM is 4.3 Å from the imidazole of His 19 of MGS. Additionally, K12 of TIM is within hydrogen bonding distance of 2PG whereas corresponding residue, His 19 of MGS does not make any interactions with 2PG.

of 2PG as is the catalytic base Glu 165 in TIM (*22*). However, Asp 71 is located on the opposite face of the 2PG-carboxylate plane from Glu 165 (Figure 4a). Since it has been shown that MGS abstracts the C3 *pro*-S proton whereas TIM abstracts the C3 *pro*-R proton, the enediol(ate) intermediate must be in the same cis-conformation as has been demonstrated for TIM. The carboxylate of Glu 165 in TIM is found in a hydrophobic environment that is thought to raise the pK_a of this general base to better match that of the C3 proton of DHAP (*38*). A similar strategy is apparent in MGS. In addition to the hydrophobic residues surrounding Asp 71 in MGS, the carboxylate group of Asp 101 is near the carboxylate group of Asp 71. Since Asp 101 is involved in a buried salt bridge with Arg 107 of a neighboring subunit, it is likely to be negatively charged. The presence of this negative charge ~5 Å away should further raise the pK_a of the Asp 71 carboxylate. The higher pK_a (6.9) of Asp 71 (unpublished data) compared to the pK_a (6.05) of Glu 165-(*39*) may give rise to a faster rate of proton abstraction and may explain, in part, the lack of a deuterium isotope effect for MGS (*6*), while one can be observed in TIM (*40*, *41*).

In addition to raising the pK_a of the carboxylate base, TIM appears to reduce the pK_a of the substrate's C3 proton by using His 95 to polarize the carbonyl of DHAP (*42*). The observation that DHAP bound to TIM is 8-fold more susceptible to $NaBH_4$ reduction than free DHAP suggests that electrophilic catalysis is occurring (*43*). His 98 of MGS is equivalently positioned with respect to the carboxylate oxygen of 2PG as is His 95 of TIM. Although approaching from different sides of the 2PG-carboxylate plane, the Nϵ2

nitrogen of the histidine is in the plane of the carboxylate of 2PG in both the MGS and TIM structures. If the mechanism for enediol(ate) formation is indeed an example of convergent evolution, it is expected that His 98 of MGS will be involved in electrophilic catalysis like its counterpart His 95 of TIM. In TIM, a third residue is also implicated in catalysis; Lys 12 of TIM appears to both polarize the carbonyl by stabilizing the charge on His 95 and attract the negatively charged phosphoryl of DHAP/GAP (*44*−*46*). The residue in MGS that most nearly mirrors Lys 12 of TIM is His 19. However, while a histidine residue at low pH has successfully replaced Lys 12 of TIM (*46*), there are some substantial differences in the relative locations of Lys 12 of TIM and His 19 of MGS. The amino group of Lys 12 is located within hydrogen-bonding distance to the carboxylate of 2PG, while His 19 of MGS is not within hydrogen-bonding distance. More importantly, the imidazole ring is not near the phosphoryl moiety of 2PG. These differences may indicate subtle differences in the catalytic mechanism which will only be understood by obtaining more mutagenic and kinetic data for MGS. However, the similarity in the positions of the carboxylate catalytic base and the imidazole catalytic electrophile in these two enzymes suggest that these two otherwise unrelated proteins have converged upon a highly efficient mechanism for enediol(ate) formation.

Recently, it has been proposed that the isomerization catalyzed by TIM can be best explained by a partition of some of the reactants to a "crisscross" mechanism of proton transfer (*47*, *48*). In this mechanism, Glu 165 abstracts the C3 proton of DHAP and then protonates the O2 oxygen of the enediolate. Glu 165 then abstracts the O3 proton and reprotonates the enediolate at the C2 position. In this mechanism, His 95 is positioned to stabilize the proposed enediol and enediolate. If this mechanism were to occur in MGS, then Asp 71 would proceed through the first three steps of the crisscross mechanism and then fail to reprotonate the enediolate at the C2 position. If DHAP is modeled on the 2PG structure, then the distance between the closest carboxylate oxygen of Asp 71 to the O2 oxygen and C2 carbon would be 4.4 and 3.7 Å, respectively. Not only are these distances too far for efficient proton transfer, but they are not consistent with a mechanism that allows protonation at O2 but does not allow protonation at C2. Thus, methylglyoxal synthase is unlikely to proceed by a truncated crisscross mechanism.

Phosphoryl Stabilization. MGS and TIM differ in that the former must catalyze the elimination of phosphate while the latter must prevent it. As noted in the uncatalyzed DHAP elimination reaction, the observed rate of phosphate elimination from the enediolate is dependent in part on the protonation state of the phosphoryl moiety (*36*). Apparently, one of the ways TIM reduces the rate of phosphate elimination is by binding to only the phosphoryl dianion. This is demonstrated by the fact that the obligate monoanion, dihydroxyacetone sulfate (DHAS), does not act as a substrate for TIM (*49*). The dependence on electrostatic forces for the binding of DHAP to TIM is readily explained by examination of the phosphoryl-binding site. In TIM, the phosphoryl-binding site is very sparse with only two possible hydrogen bonds from residues in a mobile loop to one of the phosphoryl oxygens (*50*). It has been proposed that this loop excludes bulk solvent and thus prevents undesirable side reactions (*50*). By comparison, the phosphoryl-binding site of MGS is very rich with a variety of charged and uncharged potential hydrogen bond donors and acceptors surrounding all four of the phosphoryl oxygens (Figure 2). Significantly, the conformation of the phosphoryl moiety and ligands to the phosphoryl moiety of 2PG are the same as they are found for the bound phosphate ion in the MGS formate−phosphate complex. This suggests that the phosphoryl-binding site is able to accommodate and stabilize the additional charge of the phosphate ion after elimination from DHAP. One of the potential hydrogen bond donors is the amide nitrogen of Gly 66 to the bridging oxygen of 2PG. This glycine residue is part of a highly conserved loop region [65-SGP(L/M)-GGDqQ-73] that extends from the end of β strand 4 to α helix C (Figure 2). This loop adopts an unusual conformation that connects Asp 71 with Gly 66. Gly 66 moves about 0.5 Å upon binding a phosphoryl ligand (*21*). In addition to the potential hydrogen bonds, the phosphoryl moiety is located at the amino-terminus of α helix B, which shifts position by $\sim$1 Å upon inhibitor binding. The helix dipole also contributes to the stabilization of the negative charge on the phosphoryl moiety. However, the uncatalyzed rate constant for the elimination of the enediolate dianion to the phosphate trianion is large ($k_e = 6 \times 10^6$ s^{-1}) (*37*). This suggests that methylglyoxal synthase needs only to stabilize the bound enediolate in a conformation favoring the elimination of the phosphate trianion which does not need electrostatic stabilization by the enzyme. The hydrogen bonds to the phosphoryl group may only serve to correctly position DHAP in the active site. However, the number of potential hydrogen bonds to the phosphoryl bound to this site strongly suggests that the phosphoryl moiety is being made a better leaving group as a result of binding. Mutagenesis and chemical studies are now underway to further understand the role that these residues play in catalysis.

Conformation of 2PG in TIM and MGS. It has been well documented that, for β-elimination to proceed, there must be significant overlap between the orbitals of the π-system of the double bond and the leaving group (*51*−*53*). The conformation of 2PG in both TIM and MGS is consistent with these quantum mechanical requirements. In MGS, the torsion angle around the C1−C2 bond of bound 2PG molecule brings the phosphoryl moiety out of the carboxylate plane by 60°. A model of enediol intermediate bound to MGS shows that the C1 sp^3-orbital that forms a bond with the bridging oxygen has a significant component parallel to the π orbitals of the C2−C3 double bound (Figure 5a). This alignment is consistent with MGS favoring the elimination reaction. Upon abstraction of the O3 hydroxyl hydrogen, the C3−O1P bond breaks to form a π bond with the C2 carbon and release inorganic phosphate. The fact that there are so many residues making contact with the inhibitor suggests that MGS may have evolved to bind this particular rotamer of DHAP. By contrast, in TIM the bridging oxygen is coplanar with the double bond of the enediol(ate), thus no component of the C1 sp^3-orbital that forms a bond with the bridging oxygen is parallel to the π orbitals of the C2−C3 double bound (Figure 5b). Thus, TIM minimizes the elimination reaction (*22*).

Substrate Specificity. Since MGS and TIM appear to have converged on the same mechanism to form the enediol(ate), it is interesting to consider one of the major differences

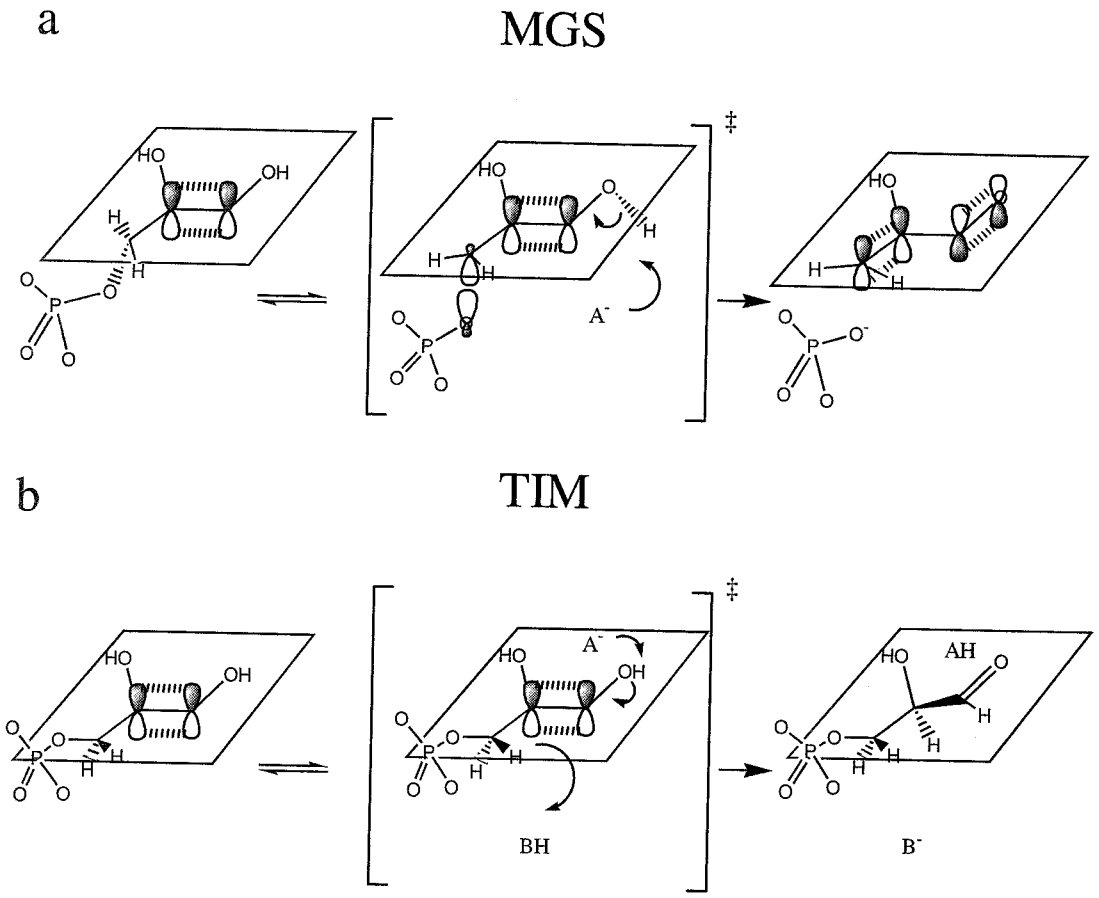

FIGURE 5: Consequence of abstracting the O3 hydroxyl hydrogen from the enediol intermediate. (a) Since the bridging phosphoryl oxygen is positioned out of the plane of the double bond in MGS, a significant component of the sp^3 orbital of C1 is aligned to form a double bond with C2 upon the abstraction of the hydroxyl hydrogen. In the transition state, the general base A is probably His 19, although His 98 cannot strictly be ruled out. (b) Since the bridging phosphoryl oxygen is positioned in the plane of the double bond in TIM, elimination is prevented, and the C2 atom rehybridizes upon protonation by BH. In the transition state, the general base A^- has been identified as His 95 and the general acid is Glu 165.

between the two enzymes. Unlike TIM, MGS is not capable of abstracting the C2 proton from GAP. This is an absolute requirement for the function of MGS, since the reverse reaction would allow MGS to form L-GAP from DHAP. L-GAP has known bactericidal activity and is known to inhibit *sn*-glycerol 3-phosphate acyltransferase and phosphatidylglycerol phosphate synthetase as well as fructose 1,6-bisphosphate aldolase (*54*−*56*). While the inability of MGS to abstract a proton from D-GAP is easily rationalized from the disposition of the catalytic base on the opposite side of the molecule from the C2 proton, the inability to abstract the C2 proton from L-GAP requires more explanation.

To better visualize the relationship among the active-site residues between MGS and TIM, the plane formed by the 2PG carboxylate was used as a mirror upon which all of the atoms of the TIM model were reflected (Figure 4b). Although the imidazole rings of His 98 of MGS and His 95 of TIM overlap, the carboxylates of Asp 71 of MGS and Glu 165 of TIM do not, the distance between Nϵ2 nitrogens of the imidazole rings and the distance between the carboxylate oxygens are of about equal magnitude (1.5 and 1.4 Å, respectively) but in opposite directions with respect to the axis of the 2PG molecule. Additionally, the χ1 torsion angle for Asp 71 places the carboxylate as close to the C2 carbon of the 2PG molecule as is possible, while changes in the χ1 torsion angle for Glu 165 would allow this residue to make a closer approach [as it does when phosphoglycolohydroxamate is bound (*38*)]. Furthermore, the χ1 torsion angle for His 98 places the Nϵ2 nitrogen as close to the O2 oxygen of the 2PG molecule as is possible, while the Nϵ2 of His 95 can make a closer approach. However, the distance between these atoms and the nearest carboxylate oxygen of 2PG are identical within experimental error. Thus, the distance from the carboxylate of Asp 71 to the C2 carbon of GAP would remain too long for efficient proton abstraction, and the distance from the Nϵ2 nitrogen of His 98 to the O1 oxygen of GAP would also be too long for efficient elecrophilic catalysis. On the basis of these observations, the rigidity and location of Asp 71 and the location and approach of His 98 must contribute to the substrate specificity.

Additional substrate specificity can be inferred from a model of L-GAP bound to the active site based on the structure of bound 2PG. This model shows that the C1 position of L-GAP would be 2.8, 3.7, and 3.4 Å from the conserved residues His 19, Phe 88, and Val 17, respectively. These distances indicate that the productive binding of L-GAP to the active site would be sterically hindered. The conserved hydrophobic residues Val 17, Phe 88, Val 102, and Leu 105 form a well-defined cavity that would prevent other phosphorylated 2-keto sugars from participating in the elimination reaction.

Modeling the Bound Enediol(ate). The structure of a subunit of MGS bound to 2PG can be superimposed on the structure of a subunit of MGS bound to formate and

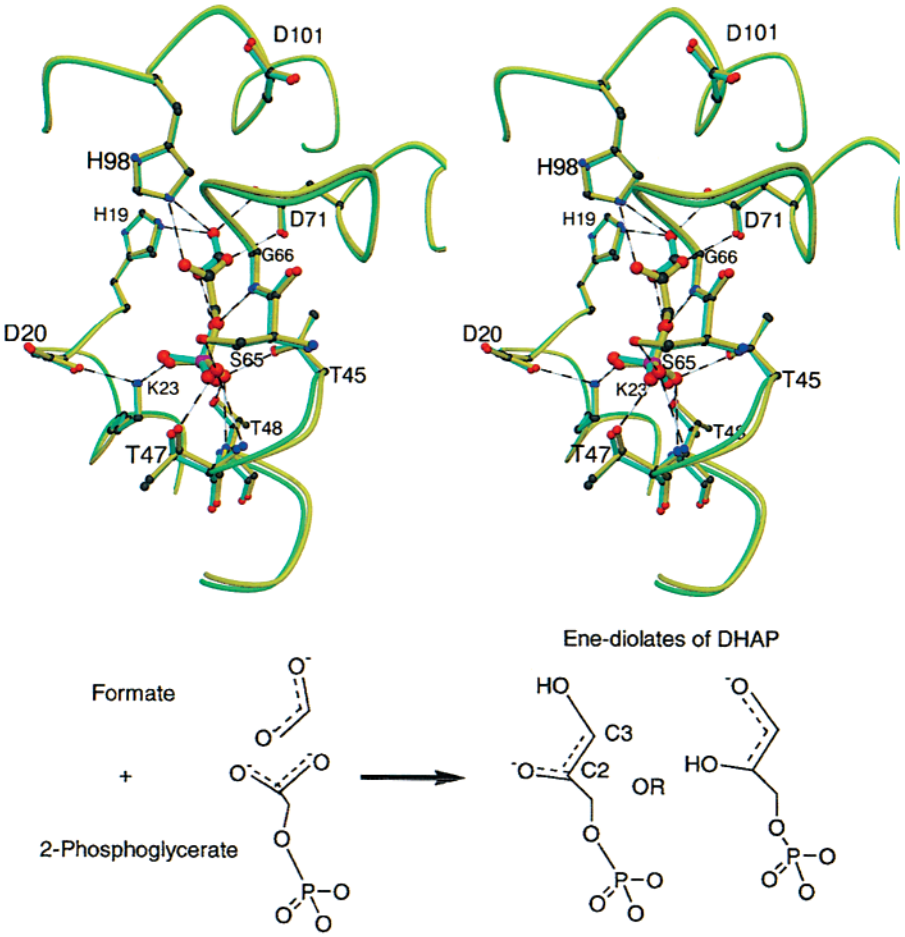

FIGURE 6: Superimposition of the MGS/formate/phosphate (green) complex with the MGS/2PG (yellow) complex. (a) The inorganic phosphate and the phosphoryl moiety of 2PG are bound to the enzyme in a nearly identical manner. One of the formate oxygens extends deeper into the active site than 2PG and makes a hydrogen bond with His 19. The second formate oxygen atom and the formate carbon atom superimpose with the carboxylate carbon and carboxylate oxygen of 2PG, respectively. (b) The resonance structures of formate and 2-phosphoglycolate are reminiscent of the resonant structures for the two possible enediolate intermediates along the methylglyoxal synthase pathway.

phosphate using only the positions of the α carbons (Figure 6a). Remarkably, this alignment shows that the carbon atom of the formate ion nearly superimposes onto one of the carboxylate oxygens of 2PG and one of the oxygens of the formate ion nearly superimposes onto the carboxylate carbon of 2PG. Fusing the two structures gives a model that has electrostatic properties that are similar to that of the transition state or to that of the bound intermediate. It is clear from these two structures that the active site can accommodate a partial negative charge on what would be the O2, C2, C3, and O3 atoms of the enediolate-like transition states (Figure 6b). However, the twist in the model (single bond character) suggests either an early-stage (substrate-like) transition state or a late-stage (product-like) transition state where the carbonyl is present. This model suggests that the there is no direct transfer of a proton from O3 to O2 of the enediolate since the distance between these two atoms is increased from the planar structure found in TIM. It is possible that His 98 assists proton transfer from O3 to O2 in addition to its role as an electrophilic catalyst as has been suggested for His 95 in TIM (*44*). However, the absolutely conserved His 19 is within hydrogen-bonding distance of the O3 oxygen of the modeled enediolate, and thus we propose that His19 may abstract the O3 hydroxyl hydrogen that initiates the collapse of the enediolate. This possibility is supported by the location of the conserved Asp 91 that could rotate about $\chi 1$ and stabilize a charge on His 19. However, it is also possible that His 19 binds to the substrate or the product, but does not participate in catalysis, since its placement is anti (rather than cis) to the phosphate leaving group.

In summary, the structure of MGS with 2PG bound strongly suggests that the mechanism of enediol(ate) formation has converged with that of TIM (Figure 7). Despite this apparent convergence, the MGS mechanism would seem to have little in common with the "loopless" TIM mutant enzyme (*57*). In "loopless" TIM, the enzyme binds DHAP, forms the enediol(ate) intermediate, and then proceeds to the isomerized product 60% of the time and falls off the enzyme the other 40% of the time. The free enediol(ate) intermediate then either reprotonates to form DHAP, D-GAP, or L-GAP or undergoes 1,4-β-elimination to form methylglyoxal and phosphate. The relative catalytic efficiency of "loopless" TIM compared to that of MGS in producing methylglyoxal is nearly 10^6 fold in favor of MGS (*7*, *57*). The structure of MGS with 2PG bound suggests that MGS achieves this efficiency both by placing the bridging phosphoryl oxygen out of the C2 plane of DHAP to optimize the orbital overlap of π bond formation and by stabilizing the phosphoryl leaving group with complementary charges, hydrogen bonds, and a helix-dipole. The relative contribution and importance of each of these factors in maintaining a faithful and efficient enzyme is currently being investigated.

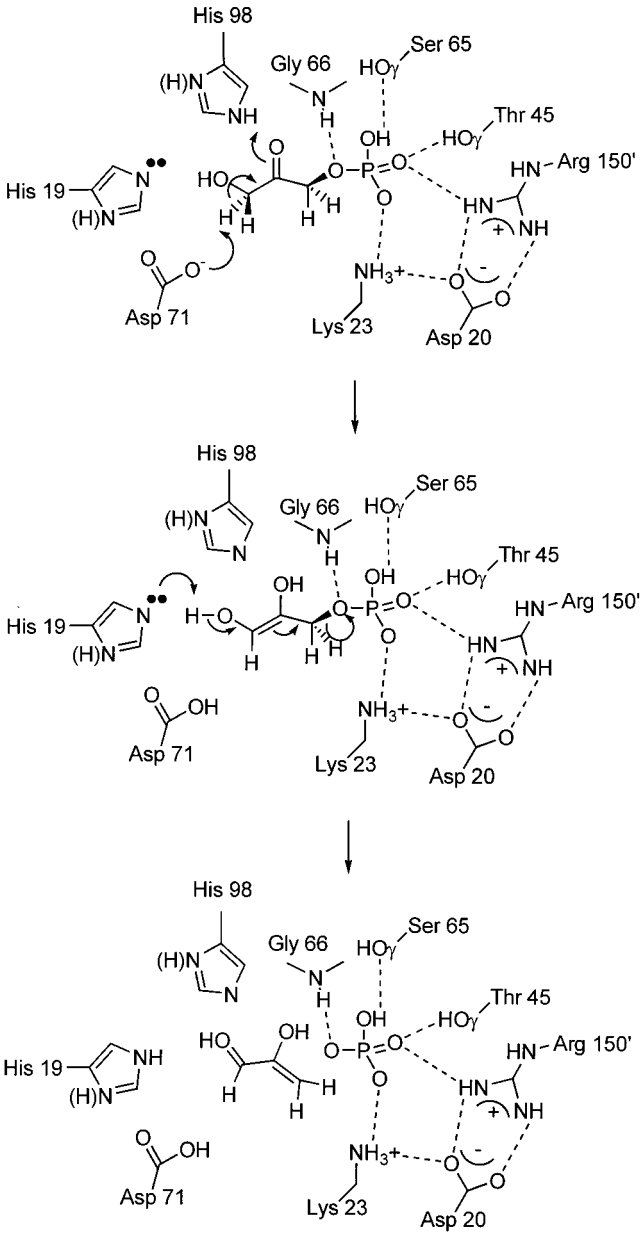

FIGURE 7: Proposed mechanism for methylglyoxal synthase. Asp 71 abstracts the *pro*-S proton from DHAP. His 98 protonates the enediolate. His 19 abstract the hydroxyl proton to initiate the 1,4-β-elimination of phosphate. The monoanionic phosphoryl is being stabilized by a number of ligands (including the hydroxyl oxygens and amide nitrogens of Thr 47 and Thr 48, not shown). Most importantly by the amide nitrogen of Gly 66 positions and stabilizes the bridging phosphoryl oxygen for bond cleavage.

ACKNOWLEDGMENTS

We are grateful to Byron Rubin, Owen Griffith, and Dagmar Ringe for their encouragement and comments on a preliminary version of this manuscript. We are also grateful to Greg Marks for providing pre-published pH-rate profile information.

REFERENCES

1. Albery, W. J., and Knowles, J. R. (1976) *Biochemistry 15*, 5631−5640.
2. Stamper, C. G., Morollo, A. A., and Ringe, D. (1998) *Biochemistry 37*, 10438−10445.
3. Sugio, S., Petsko, G. A., Manning, J. M., Soda, K., and Ringe, D. (1995) *Biochemistry 34*, 9661−9669.
4. Okamoto, A., Nakai, Y., Hayashi, H., Hirotsu, K., and Kagamiyama, H. (1998) *J. Mol. Biol. 280*, 443−461.
5. Momany, C., Ghosh, R., and Hackert, M. L. (1995) *Protein Sci. 4*, 849−854.
6. Summers, M. C., and Rose, I. A. (1977) *J. Am. Chem. Soc. 99*, 4475−4478.
7. Saadat, D., and Harrison, D. H. T. (1998) *Biochemistry 37*, 10074−10086.
8. Yuan, P. M., and Gracy, R. W. (1977) *Arch. Biochem. Biophys. 183*, 1−6.
9. Cooper, R. A., and Anderson, A. (1970) *FEBS Lett. 11*, 273−276.
10. Cooper, R. A. (1984) *Annu. Rev. Microbiol. 44*, 812−826.
11. Rahman, A., Shahabuddin, M., and Hadi, S. M. (1990) *J. Biochem. Toxicol. 5*, 161−166.
12. Papoulis, A., al-Abed, Y., and Bucala, R. (1995) *Biochemistry 34*, 648−655.
13. Baskaran, S., and Balasubramanian, K. A. (1990) *Biochem. Int. 21*, 165−174.
14. Együd, L. G., and Szent-Györgyi, A. (1966) *Proc. Natl. Acad. U.S.A. 56*, 203−207.
15. Clelland, J. D., and Thornalley, P. J. (1993) *Biochem. Soc. Trans. 21*, 160S.
16. Hopper, D. J., and Cooper, R. A. (1972) *Biochem. J. 128*, 321−329.
17. Tötemeyer, S., Booth, N. A., Nichols, W. W., Dunbar, B., and Booth, I. R. (1998) *Mol. Microbiol. 27*, 553−562.
18. Brownlee, M., and Cerami, A. (1981) *Annu. Rev. Biochem. 50*, 385−432.
19. Murthy, N. S., Bakeris, T., Kavarana, M. J., Hamilton, D. S., Lan, Y., and Creighton, D. J. (1994) *J. Med. Chem. 37*, 2161−2166.
20. Cameron, D. C., Altaras, N. E., Hoffman, M. L., and Shaw, A. J. (1998) *Biotechnol. Prog. 14*, 116−125.
21. Saadat, D., and Harrison, D. H. T. (1999) *Struct. Folding Des. 7*, 309−317.
22. Lolis, E., and Petsko, G. A. (1990) *Biochemistry 29*, 6619−6625.
23. Otwinowski, Z., and Minor, W. (1996) (Carter, C., and Sweet, R. M., Eds.) pp 307−325, Academic Press, Boston.
24. Brünger, A. T. (1992) X-PLOR Version 3.1, A system for X-ray crystallography and NMR, version 3.1, Yale University Press, New Haven, CT.
25. Brünger, A. T. (1992) *Nature 355*, 472−474.
26. Kleywegt, G. J., and Jones, T. A. (1996) *Acta Crystallogr., Sect. D 52*, 826−828.
27. Kleywegt, G. J., and Jones, T. A. (1995) *Structure 3*, 535−540.
28. Jones, T. A., Zou, J. Y., Cowan, S. W., and Kjeldgaard, M. (1991) *Acta Crystallogr., Sect. A 47*, 110−119.
29. Honig, B., Sharp, K., and Yang, A.-S. (1993) *J. Phys. Chem. 97*, 1101.
30. Nichols A., Bharadwaj, R., and Honig, B. (1993) *Biophysical 64*, 166−170.
31. Campbell, I. D., Jones, R. B., Kiener, P. A., Richards, E., Waley, S. C., and Wolfenden, R. (1978) *Biochem. Biophys. Res. Commun. 83*, 347−352.
32. Richard, J. P. (1998) *Biochemistry 37*, 4305−4309.
33. Hall, A., and Knowles, J. R. (1975) *Biochemistry 14*, 4348−4353.
34. Iyengar, R., and Rose, I. A. (1983) *J. Am. Chem. Soc. 105*, 3301−3303.
35. Richard, J. P. (1984) *J. Am. Chem. Soc. 106*, 4926−4936.
36. Richard, J. P. (1991) *Biochemistry 30*, 4581−4585.
37. Richard, J. P. (1993) *Biochem. Soc. Trans. 21*, 549−553.
38. Davenport, R. C., Bash, P. A., Seaton, B. A., Karplus, M., Petsko, G. A., and Ringe, D. (1991) *Biochemistry 30*, 5821−5826.
39. Plaut, B., and Knowles, J. R. (1972) *Biochem. J. 129*, 311−320.
40. Fisher, L. M., Albery, W. J., and Knowles, J. R. (1976) *Biochemistry 15*, 5621−5626.
41. Leadlay, P. F., Albery, W. J., and Knowles, J. R. (1976) *Biochemistry 15*, 5617−5620.

42. Komives, E. A., Chang, L. C., Lolis, E., Tilton, R. F., Petsko, G. A., and Knowles, J. R. (1991) *Biochemistry 30*, 3011−3019.
43. Webb, M. R., and Knowles, J. R. (1975) *Biochemistry 14*, 4692−4698.
44. Bash, P. A., Field, M. J., Davenport, R. C., Petsko, G. A., Ringe, D., and Karplus, M. (1991) *Biochemistry 30*, 5826−5832.
45. Joseph-McCarthy, D., Lolis, E., Komives, E. A., and Petsko, G. A. (1994) *Biochemistry 33*, 2815−2823.
46. Lodi, P. J., Chang, L. C., Knowles, J. R., and Komives, E. A. (1994) *Biochemistry 33*, 2809−2814.
47. Harris, T. K., Abeygunawardana, C., and Mildvan, A. S. (1997) *Biochemistry 36*, 14661−14675.
48. Harris, T. K., Cole, R. N., Comer, F. I., and Mildvan, A. S. (1998) *Biochemistry 37*, 16828−16838.
49. Belasco, J. G., Herlihy, J. M., and Knowles, J. R. (1978) *Biochemistry 17*, 2971−2978.
50. Alber, T. C., Davenport, R. C., Jr., Giammona, D. A., Lolis, E., Petsko, G. A., and Ringe, D. (1987) *Cold Spring Harbor Symp. Quant. Biol. 52*, 603−613.
51. Deslongchamps, P., Atlani, P., Frehel, D., and Malaval, A. (1972) *Can. J. Chem. 50*, 3405−3408.
52. Kirby, A. J. (1983) *The Anomeric Effect and Related Stereoelectronic Effects at Oxygen*, Springer-Verlag, Berlin.
53. Rose, I. A. (1981) *Philos. Trans R. Soc. London, Series B: Biol. Sci. 293*, 131−143.
54. Leoncini, G., Maresca, M., Ronchi, S., and Bonsignore, A. (1979) *It. J. Biochem. 28*, 232−244.
55. Kalyananda, M. K., Engel, R., and Tropp, B. E. (1987) *J. Bacteriol. 169*, 2488−2493.
56. Tang, C.-T., Engel, R., and Tropp, B. E. (1999) *Antimicrob. Agents Chemother. 11*, 147−153.
57. Pompliano, D. L., Peyman, A., and Knowles, J. R. (1990) *Biochemistry 29*, 3186−3194.
58. Laskowski, R. A., MacArthur, M. W., Moss, D. S., and Thornton, J. M. (1993) *J. Appl. Crystallogr. 26*, 548−558.
59. Engh, R. A. and Huber, R. (1998) *Acta Crystallogr., Sect. A 47*, 392−400.

BI992666F